Dipole transition strengths and level densities in $A \leq 80$ odd-odd nuclei obtained from thermal neutron capture

Bernd Krusche* and Klaus Peter Lieb
II. Physikalisches Institut, Universität Göttingen, D-3400 Göttingen, Federal Republic of Germany
(Received 11 August 1986)

Level densities and primary $E1$ and $M1$ transition strengths recently obtained from extensive studies in fifteen light and medium odd-odd nuclei ($20 \leq A \leq 80$) are analyzed. The level densities are parametrized in terms of the constant temperature Fermi gas and the Bethe formulae; both models provide equally good fits to the experimental results. Empirical relationships between their parameters and simple expressions for the extension of level densities and γ-ray strength functions into the region of noncomplete level schemes are proposed. For nuclei with $A \gtrsim 46$ the $E1$ strengths agree very well with the predictions of the electric giant dipole resonance model; for the lighter nuclei the $E1$ strengths are stronger than the giant dipole resonance prediction because of direct neutron capture. The observed mass and energy dependence of $M1$ strengths seems to indicate some influence of the magnetic giant dipole resonance; however, the $M1$ spectra are strongly structured by nonstatistical effects, in particular in the *sd* shell.

I. INTRODUCTION

The γ-radiation emitted after thermal neutron capture has been extensively studied in the past decades throughout the full Periodic Table. The motivations of these experiments have been either to determine the structure of low-lying states via the measurement of level energies, spins and parities, and γ-ray branching ratios, or to investigate properties of the primary γ-ray spectrum by which the capture state(s) decay(s). In general, emphasis has therefore been put either on the secondary, low energy part of the (n,γ) spectrum related to structure effects, or to the primary high energy part. In heavy nuclei, the enormous line density in the intermediate energy region, i.e., at about half the neutron binding energy E_B, has restricted the (n,γ) studies to the first 1–2 MeV of excitation. The high neutron flux and very efficient bent crystal and pair spectrometer available at the Institut Laue-Langevin (ILL) reactor, on the other hand, have allowed workers to follow the decay cascades in much detail, at least in light and medium nuclei.

Over the last five years, the Göttingen-Grenoble-Munich collaboration has provided very detailed results for the (n,γ) reactions on ^{19}F, ^{23}Na, ^{27}Al, ^{35}Cl, ^{39}K, and ^{41}K targets[1–6] leading to final odd-odd nuclei with $20 \leq A \leq 42$. In each case, some 80–99 % of the total γ-ray flux have been accommodated in the level scheme, with tens of new levels identified and spins and parities assigned. Similar studies in the mass range $32 \leq A \leq 80$ have been performed by the groups at Petten (^{46}Sc, ^{60}Co, ^{64}Cu, and ^{66}Cu; Refs. 7–10), McMaster (^{32}P, ^{56}Mn, and ^{76}As; Refs. 11–13), and some other collaborations (e.g., ^{72}Ga and ^{80}Br; Refs. 14 and 15).

This effort has therefore provided an improved and much more complete data set. It may serve as basis to test statistical models and to elucidate in what way chaotic motion in nuclei takes over for increasing excitation energy. The purpose of the present work is to analyze the recently measured data in odd-odd nuclei in the mass range $20 \leq A \leq 80$ on a common footing. Table I summarizes the investigated nuclei with their binding energy E_B, their number of levels, and their primary $E1$ and $M1$ transitions observed in the (n,γ) process. In Sec. II the density of levels will be parametrized with the Bethe formulae and the constant temperature Fermi gas model. In Sec. III the distribution function of the primary γ-ray spectrum will be analyzed, while in Sec. IV the strength of primary transitions will be discussed in detail.

II. LEVEL DENSITIES

A. Level density formulae

The statistical considerations are based on the analysis of level densities. The level density $\rho(E_x)$ at excitation energies E_x up to about 10 MeV usually is parametrized by either[24–29] the Bethe formula (BF),

$$\rho_B(E_x) = \frac{\exp[2\sqrt{a(E_x - E_1)}]}{12\sqrt{2}\sigma a^{1/4}(E_x - E_1)^{5/4}} , \tag{1}$$

or the constant temperature Fermi gas model (CTF),

$$\rho_C(E_x) = \frac{1}{T}\exp\left[\frac{E_x - E_0}{T}\right] . \tag{2}$$

Here, a denotes the single particle level density parameter, T the nuclear temperature, E_1 and E_0 the energies of the fictive ground states, and σ the spin-cutoff parameter. Defining the nuclear temperature by the equation

$$T^{-1} = \frac{d}{dE_x}\ln\rho(E_x) . \tag{3}$$

One obtains for the Bethe formula the energy dependent temperature $T_B(E_x)$:

TABLE I. Survey on odd-odd nuclei studied via the (n,γ) process.

Nucleus	I_c [a]	E_B (keV)[b]	Total number of states observed in (n,γ)	Number of primary transitions observed Total	$E1$	$M1$	Ref.[c]
^{20}F	1^+	6601.33(4)	26	20	6	11	1
^{24}Na	$1^+,2^+$	6959.73(7)	45	41	15	18	2
^{28}Al	$2^+,3^+$	7725.18(9)	50	44	8	31	3
^{32}P	$0^+,1^+$	7935.70(4)	32	28	11	12	11,16
^{36}Cl	2^+	8579.68(9)	75	67	26	26	4
^{40}K	$1^+,2^+$	7799.55(8)	63	50	23	10	5
^{42}K	$1^+,2^+$	7533.82(8)	134	122	24	5	6
^{46}Sc	$3^-,4^-$	8760.77(14)	133	124	16	18	7,17
^{56}Mn	$2^-,3^-$	7270.8(5)	81	80	28	11	12,18
^{60}Co	$3^-,4^-$	7491.92(8)	144	117	30	12	8
^{64}Cu	$1^-,2^-$	7916.09(12)	110	82	22	3	9,19
^{66}Cu	$1^-,2^-$	7065.97(11)	100	91	20	4	10,20
^{72}Ga[d]	$1^-,2^-$	6519(1)	84	84	9	10	14,21
^{76}As	$1^-,2^-$	7329(2)	120	120	14	13	13,22
^{80}Br[e]	$1^-,2^-$	7892.35(20)	72	77	15	3	15,23

[a] Spin and parity of capture state(s).
[b] Neutron binding energy.
[c] First reference refers to (n,γ) work, the second to additional information on spins, parities, etc.
[d] Intensities normalized by present authors.
[e] Strong transitions with $E_\gamma > 5$ MeV taken as primary if unassigned.

$$T_B(E_x)=\frac{E_x-E_1}{\sqrt{a(E_x-E_1)}-\frac{3}{2}} . \tag{4}$$

Both formulae refer to the total level density of a nucleus; however, only states within a certain spin window are populated by the thermal (n,γ) reaction. The partial level density $\rho(E_x,J)$ of states with spin J and parity $\pi=\pm$ follows from the spin distribution, which is given in terms of the spin-cutoff parameter:[30]

$$\rho(E_x,J)=f(J)\rho(E_x) , \tag{5a}$$

$$f(J)=\exp\left[-\frac{J^2}{2\sigma^2}\right]-\exp\left[-\frac{(J+1)^2}{2\sigma^2}\right] \approx \frac{2J+1}{2\sigma^2}\exp\left[-\frac{(J+\frac{1}{2})^2}{2\sigma^2}\right] . \tag{5b}$$

Consequently, the density $\rho(E_x,J_1,J_2)$ of states in the spin range $J_1 \leqq J \leqq J_2$ can be written as

$$\rho(E_x,J_1,J_2)=\sum_{J=J_1}^{J_2} f(J)\rho(E_x) = \left\{\exp\left[-\frac{J_1^2}{2\sigma^2}\right]-\exp\left[-\frac{(J_2+1)^2}{2\sigma^2}\right]\right\}\rho(E_x) . \tag{6}$$

The spin-cutoff parameter σ can be estimated in the framework of the BF model by[26]

$$\sigma^2 \approx 0.0888 A^{2/3}\sqrt{a(E_x-E_1)} . \tag{7}$$

The dependence of σ on the excitation energy E_x is weak [$\sigma \sim (E_x-E_1)^{1/4}$]; thus a constant σ value may be used for the CTF model.

The integrated number of states $N(E_x)$ below the excitation energy E_x is often used to compare experimental results to these parametrizations. By means of

$$N(E_x)=\int_0^{E_x}\rho(E')dE' , \tag{8}$$

one obtains

$$N_C(E_x,J_1,J_2)=\left\{\exp\left[-\frac{J_1^2}{2\sigma^2}\right]-\exp\left[-\frac{(J_2+1)^2}{2\sigma^2}\right]\right\} \times\left[\exp\left[\frac{E_x-E_0}{T}\right]-\exp\left[-\frac{E_0}{T}\right]\right] \tag{9}$$

for the CTF model. The corresponding $N_B(E_x,J_1,J_2)$ value of the BF model is obtained by numerical integration. The level density at very low excitation energies is dominated by structure effects which are not included in any of the above formulae. Consequently, discrepancies between the experimental and fitted integrated number of states may occur. These nonstatistical low energy effects are compensated for by the parameter N^0 introduced in the following way:

$$N^{\text{expt}}(E_x,J_1,J_2)=N(E_x,J_1,J_2)+N^0 . \tag{10}$$

TABLE II. Level density parameters.

Nucleus	Spin window (n,γ)	Spin window resonances	Resonance spacing[a] (keV)	Fit region (MeV)	Bethe formula[b] a (MeV^{-1})	Bethe formula[b] E_1 (MeV)	CTF[c] T (MeV)	CTF[c] E_0 (MeV)
^{20}F	$(0-2)^{\pm}$	$0,1,2^-$	32(5)	0–3.0	2.22(11)	−3.5(4)	3.1(3)	−6.7(6)
^{24}Na	$(0-3)^{\pm}$	$0^-,1,2,3^-$	30(6)	0–4.0	2.85(8)	−2.4(3)	2.40(15)	−4.5(5)
^{28}Al	$(1-4)^{\pm}$	$1^-,2,3,4^-$	24(3)	0–4.0	2.84(8)	−2.8(3)	2.40(12)	−4.4(5)
^{32}P	$(0-2)^{\pm}$			0–3.0	2.8(3)	−2.8(5)	2.7(3)	−5.4(10)
^{36}Cl	$(1-3)^{\pm}$	$0^-,1,2,3^-$	13(4)	0–3.0	3.12(7)	−2.3(3)	2.26(10)	−3.6(5)
^{40}K	$(0-3)^{\pm}$	$0^-,1,2,3^-$	4.3(5)	1.5–3.5	4.52(10)	−1.5(3)	1.77(8)	−3.6(5)
^{42}K	$(0-3)^{\pm}$	$0^-,1,2,3^-$	3.0(4)[d]	0–2.5	4.54(10)	−2.6(3)	1.78(8)	−4.6(5)
^{46}Sc	$(2-5)^{\pm}$	$3^-,4^-$	1.1(2)	0.5–2.5	6.44(15)	−1.30(15)	1.28(5)	−2.8(3)
^{56}Mn	$(1-4)^{\pm}$	$2^-,3^-$	1.9(5)[e]	0.5–2.5	7.28(15)	−0.4(1)	1.12(4)	−1.7(4)
^{60}Co	$(2-5)^{\pm}$	$3^-,4^-$	1.4(2)	0–2.5	6.77(20)	−1.47(15)	1.22(6)	−2.9(4)
^{64}Cu	$(0-3)^{\pm}$	$1^-,2^-$	0.62(7)	0–2.0	7.76(15)	−1.0(2)	1.12(4)	−2.5(5)
^{66}Cu	$(0-3)^{\pm}$	$1^-,2^-$	1.0(2)	0.5–3.0	8.62(20)	−0.05(10)	0.98(4)	−1.3(4)
^{72}Ga	$(0-3)^{\pm}$	$1^-,2^-$	0.37(5)[e]	0–1.5	8.92(25)	−1.8(3)	1.03(4)	−3.6(5)
^{76}As	$(0-3)^{\pm}$	$1^-,2^-$	0.087(10)[e]	0–1.0	9.92(25)	−1.8(3)	0.98(6)	−3.8(5)
^{80}Br	$(0-3)^{\pm}$	$1^-,2^-$	0.06(3)[e]	0–1.5	10.24(30)	−1.25(30)	0.92(6)	−3.0(4)

[a] Reference 32, unless otherwise stated.
[b] a and E_1 defined in Eq. (1).
[c] T and E_0 defined in Eq. (2).
[d] Reference 32; corrected for missing resonances.
[e] Reference 28.

B. Fit of level density parameters

In the present study the density of states accessible by primary dipole transitions from the capture state was used to fit the level density parameters. In this spin window the level schemes are essentially complete up to a certain excitation energy called the "limit of completeness" (see below). The experimental density was obtained by counting the states within proper energy bins, 1 MeV wide for the lightest nuclei and 0.5 MeV wide for the others. As usual, the density of these states at the neutron binding energy E_B was extrapolated from the level spacing of s (p) -neutron resonances using [Eqs. (5)]. The values of σ given in Ref. 26 were used for this transformation. Note that it depends only weakly on σ because the spin windows are similar.[31]

A least squares fit including the density of states below the limit of completeness and at the neutron binding energy was used to adjust the parameters χ^2 being defined as

$$\chi^2 := \frac{[\rho(E_B,J_1,J_2)-\rho_R]^2}{(\Delta\rho_R)^2} + \sum_{i=n}^{k} \frac{[\rho(E_i,J_1,J_2)-\rho_i]^2}{(\Delta\rho_i)^2} \ . \tag{11}$$

Here, $\rho_R \pm \Delta\rho_R$ denotes the density from resonance spacings, E_i the center of the ith bin, ρ_i the respective level density, and $n \le i \le k$ the intervals defined in Table II. The weights $(\Delta\rho_i)^2$ were taken as proportional to ρ_i^{-1}.

All essential input values to the fitting procedure and the deduced level density parameters are summarized in Table II.

C. Discussion of results

The experimental level densities and $N(E_x)$ values of the isotopes ^{36}Cl and ^{56}Mn are compared to the CTF and BF fits in Fig. 1. Obviously, the neutron resonance density and the density of states below a critical energy (≈ 5.5 MeV for ^{36}Cl, ≈ 3 MeV for ^{56}Mn) are reproduced very well by the fits. We conclude that up to this energy the level schemes are rather complete, whereas above this energy more and more states escape detection (for a detailed discussion, see Sec. III B). The agreement between the experimental values and fitted curves does not favor any of the level density formulae. The average χ^2 values of the CTF ($\bar{\chi}^2_C = 1.35 \pm 0.20$) and BF fits ($\bar{\chi}^2_B = 1.42 \pm 0.30$) agree very well. We thus conclude that both models are appropriate up to the neutron binding energy, with the understanding that the parameters are properly adjusted.

When comparing the parameters obtained for the two level density formulae a simple relationship emerges:

$$E_1 - E_0 = 1.67 \pm 0.11 \text{ MeV} \ , \tag{12a}$$

$$T = \frac{\frac{2}{3}E_B - E_1}{[a(\frac{2}{3}E_B - E_1)]^{1/2} - \frac{3}{2}} (1.00 \pm 0.01) \ , \tag{12b}$$

i.e., the positions of the fictive ground states differ only by a constant value and the temperature T of the CTF model equals the temperature obtained from the BF model at $\frac{2}{3}$ the neutron binding energy E_B.

The level density parameters a and E_1 are displayed in Fig. 2 as a function of the mass number A. The rather smooth mass dependence allows one to estimate their values for other odd-odd nuclei in this mass region. The

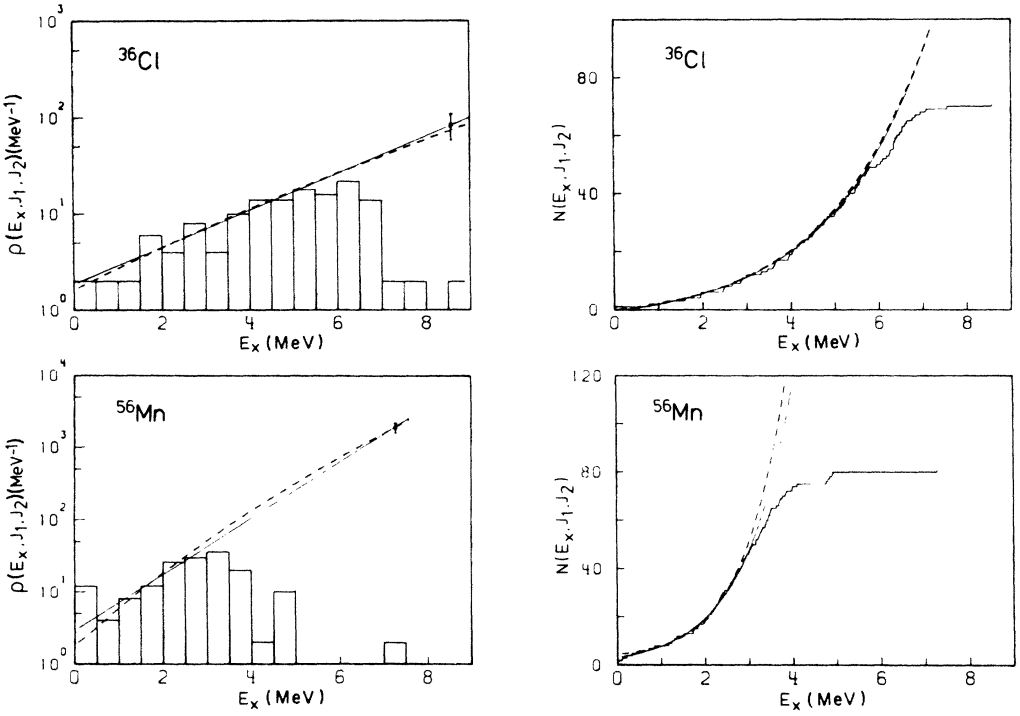

FIG. 1. Level density $\rho(E_x,J_1,J_2)$ and integrated number of levels $N(E_x,J_1,J_2)$ in the isotopes ^{36}Cl and ^{56}Mn determined in the (n,γ) process. Histograms, experimental values; solid lines, CTF fits; dashed lines, Bethe formula.

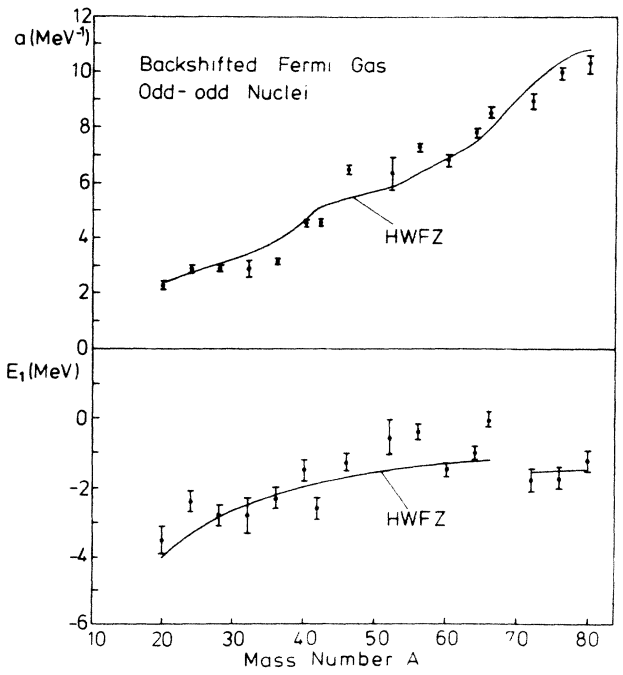

FIG. 2. Fitted level density parameters a and E_1 vs the mass number A. The lines indicate the semiempirical values of Holmes *et al.* (Ref. 33).

often used semiempirical calculations of Holmes *et al.*[33] are given for comparison. The overall trend is well reproduced; however, the "step" of the parameter a around the $A=40$ shell closure is much more pronounced for the fitted values. As discussed by Rohr,[34] these steps are due to successive collisions in the compound process because the level density increases as more nucleons are excited. The $A\approx 40$ step corresponds to the appearance of 3p2h states; the second one around $A\approx 70$ to 4p3h states. Since the investigated nuclei are odd-odd ones, no pairing energy contribution to the ground state shifts is expected. The negative values of the fictive ground states E_0 and E_1 reflect the fact that in this mass region both the BF and CTF models have to be further "backshifted."

The discussion of the primary γ-ray spectrum presented in the following sections is based on the CTF parametrization of the level density because its mathematical simplicity yields analytical solutions for most integrations involved.

III. DISTRIBUTION OF PRIMARY TRANSITIONS

A. Energy dependence and fluctuations

In this section we discuss the spectrum of primary dipole transitions. At this stage we do not divide it into $E1$ and $M1$ components. Since the γ-ray flux connected with transitions of higher multipolarities is negligible in most nuclei, we are talking about the total primary spectrum.

From a statistical point of view, the shape of this spectrum depends on the density of final states, the energy scaling of the average intensity, and the fluctuations with respect to this average. All γ-transition intensities are given in "photons per 100 captured neutrons" ("%") throughout this paper.

The integrated intensity of primary transitions

$$Y(E_x)=\sum_{E_B-E_x<E_\gamma} I_\gamma(E_\gamma) \tag{13}$$

is best suited to determine the average energy dependence. In the statistical model the quantity $Y(E_x)$ is given by

$$Y(E_x)=\int_0^{E_x}\rho(E',J_1,J_2)b(E_B-E')dE' , \tag{14}$$

where the average intensity $b(E_\gamma)$ of primary dipole transitions is normalized as to make $Y(E_B)=100\%$, and the spin window of states accessible by these transitions is defined by J, $J_1\leqq J\leqq J_2$. The level densities from (n,γ) experiments at higher excitation energies are strongly underestimated due to detection probability effects, but the level schemes are essentially complete in the low energy region. Thus nonstatistical effects influencing $\rho(E_x,J_1,J_2)$ may be included by using experimental level densities at low excitation energies; on the other hand, the CTF parametrization is used in the noncomplete high energy region.

The single particle approach[35] yields a $b(E_\gamma)\sim E_\gamma^3$ scaling for both $E1$ and $M1$ transitions. On the other hand, taking into account the giant dipole resonance (GDR), a different energy dependence is expected. Simplified global estimates[36,37] propose $b(E_\gamma)\sim E_\gamma^5$ for high energy $E1$ and $M1$ transitions dominated by the GDR. This behavior is indeed experimentally found for $E1$ transitions in heavy nuclei. The situation is less clear in light nuclei and for $M1$ transitions. In heavy nuclei the primary spectrum is dominated by $E1$ transitions, whereas for light nuclei the influence of the GDR decreases. Nevertheless, an E_γ^5 scaling was reported for the nucleus ^{46}Sc even though a considerable fraction of the primary flux was assigned to $M1$ transitions.[7]

With this in mind, we compared the experimental integrated intensities $Y(E_x)$ obtained from Eq. (13) to the statistical prediction [Eq. (14)] using

$$b(E_\gamma)=\overline{r}_{(n)}E_\gamma^n \quad \text{with } n=3 \text{ or } 5 . \tag{15}$$

The relative average strengths $\overline{r}_{(n)}$, $n=3,5$, may be obtained either by averaging,

$$\overline{r}_{(n)}=\overline{(I_\gamma E_\gamma^{-n})} , \tag{16}$$

or from the normalization condition $Y(E_B)=100\%$. In the first case only primary transitions populating states in the "complete" region may be included. As especially in the heavier nuclei detection probability effects cut the primary spectrum at relative low excitation energies, the second method is much more reliable.

The most suitable exponents of the energy scaling and the corresponding $\overline{r}_{(n)}$ values determined by both methods are given in Table III. The experimental and theoretical curves of $Y(E_x)$ with $n=3$ or 5 for the nuclei ^{28}Al, ^{42}K, and ^{66}Cu are sampled in Fig. 3. The results suggest the following division of the investigated nuclei into three groups.

(i) The isotopes with $20\leq A\leq 32$: The experimental spectra do not agree with the statistical assumptions either assuming E_γ^3 or E_γ^5 scaling; the discrepancies are most significant for ^{20}F and decrease with increasing mass number A.

(ii) The isotopes with $36\leq A\leq 42$: The spectra are best reproduced by the E_γ^3 energy scaling.

(iii) The isotopes with $46\leq A\leq 80$: the suitable energy dependence is given by E_γ^5.

These three classes therefore represent a transition from nonstatistical behavior to the E_γ^5-scaling law typical for primary spectra dominated by the GDR. However, this

TABLE III. Energy scaling and parameters of Thomas-Porter fluctuations.

Nucleus	Exponent n	$\overline{r}_{(n)}$ (MeV^{-n}) b	c	Number of degrees of freedom ν
^{20}F	3[a]	5.6×10^{-2}	7.1×10^{-2}	2.9(13)
^{24}Na	3[a]	4.7×10^{-2}	4.4×10^{-2}	1.0(3)
^{28}Al	3[a]	2.2×10^{-2}	2.3×10^{-2}	1.1(3)
^{32}P	3[a]	2.4×10^{-2}	2.6×10^{-2}	0.7(3)
^{36}Cl	3	1.4×10^{-2}	1.5×10^{-2}	1.8(4)
^{40}K	3	1.7×10^{-2}	1.2×10^{-2}	2.9(7)
^{42}K	3	0.84×10^{-2}	0.71×10^{-2}	1.9(4)
^{46}Sc	5	7.7×10^{-4}	6.3×10^{-4}	2.0(4)
^{56}Mn	5	3.6×10^{-4}	3.5×10^{-4}	1.8(4)
^{60}Co	5	1.8×10^{-4}	1.6×10^{-4}	1.7(3)
^{64}Cu	5[a]	1.2×10^{-4}	1.1×10^{-4}	1.3(3)
^{66}Cu	5	3.8×10^{-4}	4.0×10^{-4}	1.2(2)
^{72}Ga	5	1.2×10^{-4}	1.2×10^{-4}	1.6(3)
^{76}As	5	0.34×10^{-4}	0.31×10^{-4}	2.0(3)
^{80}Br	5	0.18×10^{-4}	0.23×10^{-4}	1.8(5)

[a] Strong nonstatistical effects.
[b] Calculated according to Eq. (16).
[c] Calculated from $Y(E_B)=100$.

global inspection does not allow us to determine the physical reasons behind this, such as level density effects (e.g., different distributions of positive and negative parity states), changes in the energy dependence of $E1$ and/or $M1$ strengths, changes in the relative fractions of $E1$ and $M1$ transitions, and nonstatistical effects. The detailed discussion of $E1$ and $M1$ strengths in Sec. IV will shed light on this question.

Once the appropriate energy scaling is established, it is possible to investigate the fluctuations of the individual energy reduced intensities $r_i = I_i E_i^{-n}$ around their average $\bar{r}_{(n)}$, where E_i denotes the γ-ray energy of the ith primary transition and I_i the intensity, respectively. The Porter-Thomas (PT) assumption of locally normally distributed matrix elements yields the well-known distribution law[38]

$$P_\nu(r)dr = \rho\Gamma(\rho)^{-1}\left[\rho\frac{r}{\bar{r}_{(n)}}\right]^{\rho-1}\exp\left[-\rho\frac{r}{\bar{r}_{(n)}}\right]dr\ , \qquad (17)$$

where $\Gamma(\rho)$ is the gamma function and $\nu = 2\rho$ the number of degrees of freedom. As to the (n,γ) reaction, this dis-

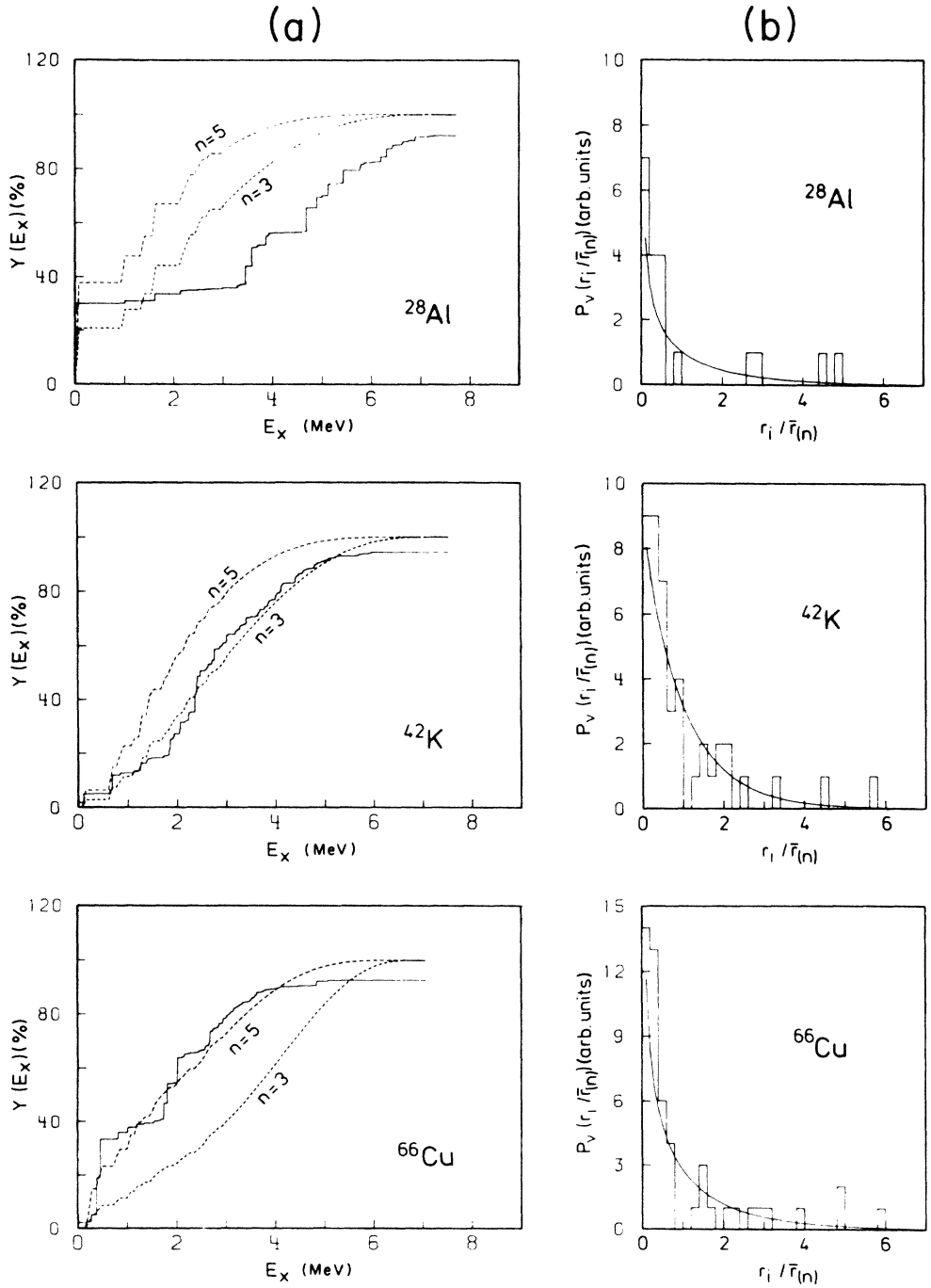

FIG. 3. (a) Integrated yield $Y(E_x)$ and (b) intensity fluctuations of primary transitions in ^{28}Al, ^{42}K, and ^{66}Cu. (a) Solid lines, experimental intensities $Y(E_x)$; dashed lines, statistical model predictions for $n = 3$ and 5. (b) Experimental and fitted Porter-Thomas distributions.

tribution function was mainly used to analyze the decay of an ensemble of resonances to the same final state. However, some authors (e.g., Ref. 39) successfully applied it to the inverse situation and in the random matrix theory (see, e.g., Ref. 40) the large scope of this concept is pointed out. Furthermore, shell-model calculations for some *sd*-shell nuclei have shown that, taking into account a proper secular behavior, the matrix elements of electromagnetic transition operators are locally normally distributed.[41]

In the most simple case the neutron capture proceeds via a single resonance (with defined spin and parity) and only one type of radiation (e.g., $E1$ transitions), in this case $\nu=1$, is expected. In the more general case of an odd-A target nucleus, resonances with spin $J=J_T\pm\frac{1}{2}$ (J_T being the ground state spin of the target nucleus) and/or $E1$ and $M1$ transitions may contribute, giving $\nu\approx 1-3$. The best value of ν was calculated from the measured energy reduced intensities r_i by the maximum likelihood method as a solution of the equation[38]

$$0=\frac{1}{m}\sum_{i=1}^{m}\ln\left[\frac{r_i}{\overline{r}_{(n)}}\right]+F(m\rho)-F(\rho)+\ln\left[1-\frac{1}{m\rho}\right], \tag{18}$$

$F(\rho)=(d/d\rho)\ln\Gamma(\rho)-\ln\rho$, and Γ is the gamma function, which accounts for finite sample size effects. Again, only transitions to final states in the "complete" region were included. The ν values are listed in Table III. They vary indeed in the range $\nu\approx 1-3$.

The experimental distributions were calculated by counting $r_i\overline{r}_{(n)}^{-1}$ in bins of 0.2 width. They are compared in Fig. 3 for some nuclei to the PT distribution with the fitted number of degrees of freedom. Obviously, the experimental distributions agree very well with the PT distribution. This is true even for the light nuclei, although their primary spectra agree very poorly with the E_γ^3 scaling used to calculate the energy reduced intensities. The discrepancies between experimental and theoretical curves of $Y(E_x)$ are mainly caused by local correlations of the transition strengths which cancel as transition over a large energy range are included. It is mainly this effect which allows one to describe the strength of $E1$ transitions over a large energy range and for many nuclei by a simple distribution function based on the GDR formalism and PT fluctuations.[42] Consequently, the investigation of structural effects is only possible if the transition strength is treated as a function of energy and/or mass number. These functions are strongly influenced by detection probability effects, which will be studied in the next section.

Finally, we would like to mention that, on the basis of these simple assumptions on level densities, level spacing distributions,[29] average energy scaling, and PT fluctuations, the complete γ-ray spectrum (also including secondary transitions) can be reproduced almost perfectly by a Monte Carlo simulation.[31,43]

B. Extension to noncomplete region

The level schemes extracted from the (n,γ) spectra are incomplete at higher excitation energies. This is caused mainly by the smaller intensities of primary transitions due to the reduced phase space. Primary transitions of a few MeV either fall in a region of many strong secondary transitions or even below the detection limit. Since the individual intensities fluctuate around the average, no sharp limit exists; however, the lower the γ-ray energy the less the parent distribution is represented by the measured transitions. In the range between completeness (typical 3–5 MeV excitation) and the neutron binding energy, we propose the following correction for the quantities $\rho(E_x)$, $\overline{r}(E_x)=\langle I_\gamma E_\gamma^{-n}\rangle$, and $Y(E_x)$.

The correction is based on the following assumptions.

(i) The average energy dependence is given by

$$b(E_\gamma)=\overline{r}_{(n)}E_\gamma^n .$$

(ii) The fluctuations can be described by the PT distribution $P_\nu(r)dr$.

(iii) The probability of detecting a primary transition with energy E_γ and intensity I_γ (and, respectively, the energy reduced intensity r) is given by

$$\epsilon(rE_\gamma^n,E_x)=\epsilon(I_\gamma,E_x),\quad E_x=E_B-E_\gamma .$$

It is more suitable to parametrize ϵ as function of E_x rather than E_γ. This simplifies the comparison of different isotopes.

Defining the correction functions by

$$\begin{aligned}
&\text{(i)}\ \ \rho_{\text{expt}}(E_x)=W(E_x)\rho(E_x) ,\\
&\text{(ii)}\ \ \overline{r}_{\text{expt}}(E_x)=V(E_x)\overline{r}(E_x) ,\\
&\text{(iii)}\ \ \frac{d}{dE_x}Y_{\text{expt}}(E_x)=U(E_x)\frac{d}{dE_x}Y(E_x) ,\\
&\text{(iv)}\ \ Y_{\text{expt}}(E_x)=\int_0^{E_x}U(E')\frac{d}{dE'}Y(E')dE' ,
\end{aligned} \tag{19a}$$

one finds

$$\begin{aligned}
&W(E_x)=\int_0^\infty P_\nu(r)\epsilon(r(E_B-E_x)^n,E_x)dr ,\\
&U(E_x)=\overline{r}_{(n)}^{-1}\int_0^\infty P_\nu(r)\epsilon(r(E_B-E_x)^n,E_x)dr ,\\
&V(E_x)=U(E_x)W(E_x)^{-1} .
\end{aligned} \tag{19b}$$

Here the experimental quantities are labeled by expt. Note that $U(E_x)$ and $W(E_x)$ approach zero for high excitation energies. The response function $\epsilon(I_\gamma,E_x)$ was parametrized in the following way (see Fig. 4):

$$\epsilon(I_\gamma,E_x)=\begin{cases}0, & I_\gamma<b_m\\ \dfrac{I_\gamma-b_m}{b_s(E_x)-b_m}, & b_m<I_\gamma<b_s(E_x)\\ 1, & b_s(E_x)<I_\gamma\end{cases} \tag{20a}$$

where

$$b_s(E_x)=\begin{cases}b_m, & E_x<E_L\\ b_m\dfrac{E_u-E_x}{E_u-E_L}+b_u\dfrac{E_x-E_L}{E_u-E_L}, & E_x>E_L .\end{cases} \tag{20b}$$

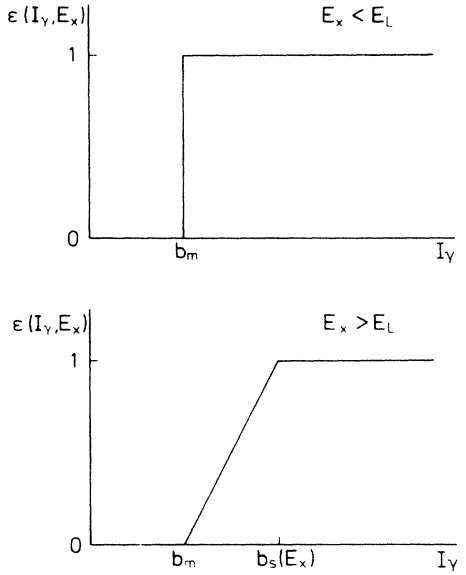

FIG. 4. Response function $\epsilon(I_\gamma, E_x)$ defined in the text.

This ansatz reflects the following considerations.

(i) The experimental detection limit b_m accounts for the spectrometer efficiency, neutron flux, amount of target material, cross section, and measuring time. It is estimated by the intensity of the weakest primary transitions detected in the experiment. High energy transitions are thus detected if their intensity exceeds the critical value b_m.

(ii) The situation is more complicated for low energy primary transitions. This part of the (n,γ) spectra is very complex and may contain unresolved doublets involving weak primary and strong secondary transitions. Furthermore, the low energy primary transitions are identified among the numerous secondary transitions by application of the Ritz combinatorial principle. A detailed discussion of these effects is given in Ref. 31. An energy dependent intensity limit $b_s(E_x)$ is introduced so that primary transitions with $b_s(E_x) < I_\gamma$ are definitely detected, while those with $I_\gamma < b_m$ are definitely not detected. For primary transitions with branching ratios $b_m < I_\gamma < b_s(E_x)$ the detection probability is linearly interpolated, as shown in Fig. 4. The function $b_s(E_x)$ equals b_m below the energy E_L and is taken as a linear function of E_x above E_L [see Eq. (20b)]. The parameters b_m, E_L, and $b_s(E_u)$ used for the detection correction are summarized in Table IV. Additionally, the excitation energies for which $W(E_x)=0.90$ and 0.10 are given. The first of these energies essentially defines the "limit of completeness" of each level scheme. In most nuclei studied the intensity of the weakest detectable primary transition is $b_m \approx 0.05\%$. However, since the level density of the heavier nuclei is much higher than for the lighter ones, the number of transitions below this limit increases considerably with mass number. Consequently, the limit of completeness decreases from about 4 MeV in the light nuclei to only 0.5 MeV for ^{76}As and ^{80}Br.

In Fig. 5 the correction functions of $\rho(E_x)$, $(d/dE_x)Y(E_x)$, $Y(E_x)$, and $\bar{r}(E_x)$ are displayed for the isotopes ^{42}K and ^{76}As. The experimental values of $\rho(E_x)$, $(d/dE_x)Y(E_x)$, and $Y(E_x)$ are compared to the statistical model predictions without and with detection probability effects included. The experimental and corrected experimental values of $\bar{r}(E_x)$ are plotted in comparison with the constants $\bar{r}_{(3)}$ and $\bar{r}_{(5)}$ for ^{42}K and ^{76}As, respectively. Obviously, the detection correction brings about excellent agreement between experiment and theory.

TABLE IV. Parameters of detection correction and "limit of completeness" defined in Eqs. (19).

Nucleus	b_m (%)[a]	b_s (%)[b]	E_L (MeV)[c]	E_x(90%) (MeV)[d]	E_x(10%) (MeV)[e]
^{20}F	0.10	0.25	2.0	3.1	5.4
^{24}Na	0.02	0.30	2.0	4.1	5.8
^{28}Al	0.05	0.35	2.0	3.8	6.1
^{32}P	0.07	0.35	2.0	3.9	6.2
^{36}Cl	0.01	0.08	4.0	5.3	7.3
^{40}K	0.20	1.40	3.5	3.0	5.2
^{42}K	0.05	0.35	2.5	3.0	5.4
^{46}Sc	0.13	0.40	2.5	1.8	4.5
^{56}Mn	0.06	0.70	2.5	2.6	4.2
^{60}Co	0.03	0.65	2.0	2.3	4.2
^{64}Cu	0.06	1.10	1.5	1.8	3.8
^{66}Cu	0.06	0.65	2.5	2.7	4.1
^{72}Ga	0.07	1.00	1.0	1.1	2.7
^{76}As	0.04	0.80	0.5	0.5	2.5
^{80}Br	0.04	1.15	1.3	0.5	2.6

[a] Intensity of weakest detectable primary transition per 100 neutrons.
[b] Intensity of weakest primary transition definitely detectable at $E_x = E_u = 5$ MeV.
[c] Excitation energy below which $b_m = b_s(E_x)$.
[d] 90% detection limit of levels.
[e] 10% detection limit of levels.

Once the suitable response function is defined by the parameters listed in Table IV, the correction easily can be extended to average $E1$ and $M1$ strengths, etc. in the following way: As a first step the experimental curves of $Y(E_x)$, restricted to $E1$ and $M1$ transitions, respectively, are compared to the statistical predictions derived from different energy scalings $n=3$ or 5. This comparison is influenced very little by detection effects. Once the average energy dependence is established, the correction factors are calculated from Eqs. (19). These corrections were applied to all transition strengths discussed in the following section.

IV. DIPOLE RADIATIVE STRENGTHS

A. Theoretical discussion and data analysis

In this section we discuss, individually, the average radiative width of primary $E1$ and $M1$ transitions. Following the notation of Bartholomew,[44] $\bar{\Gamma}^{J^\pi}_{\gamma\lambda f}(X1)$ denotes the average width of γ radiation with multipolarity $X1$ and energy E_γ depopulating a resonance with spin J and parity π to a final state E_f. Blatt and Weisskopf[35] established the well known single particle estimate assuming an equal distribution of single particle configurations on highly excited states:

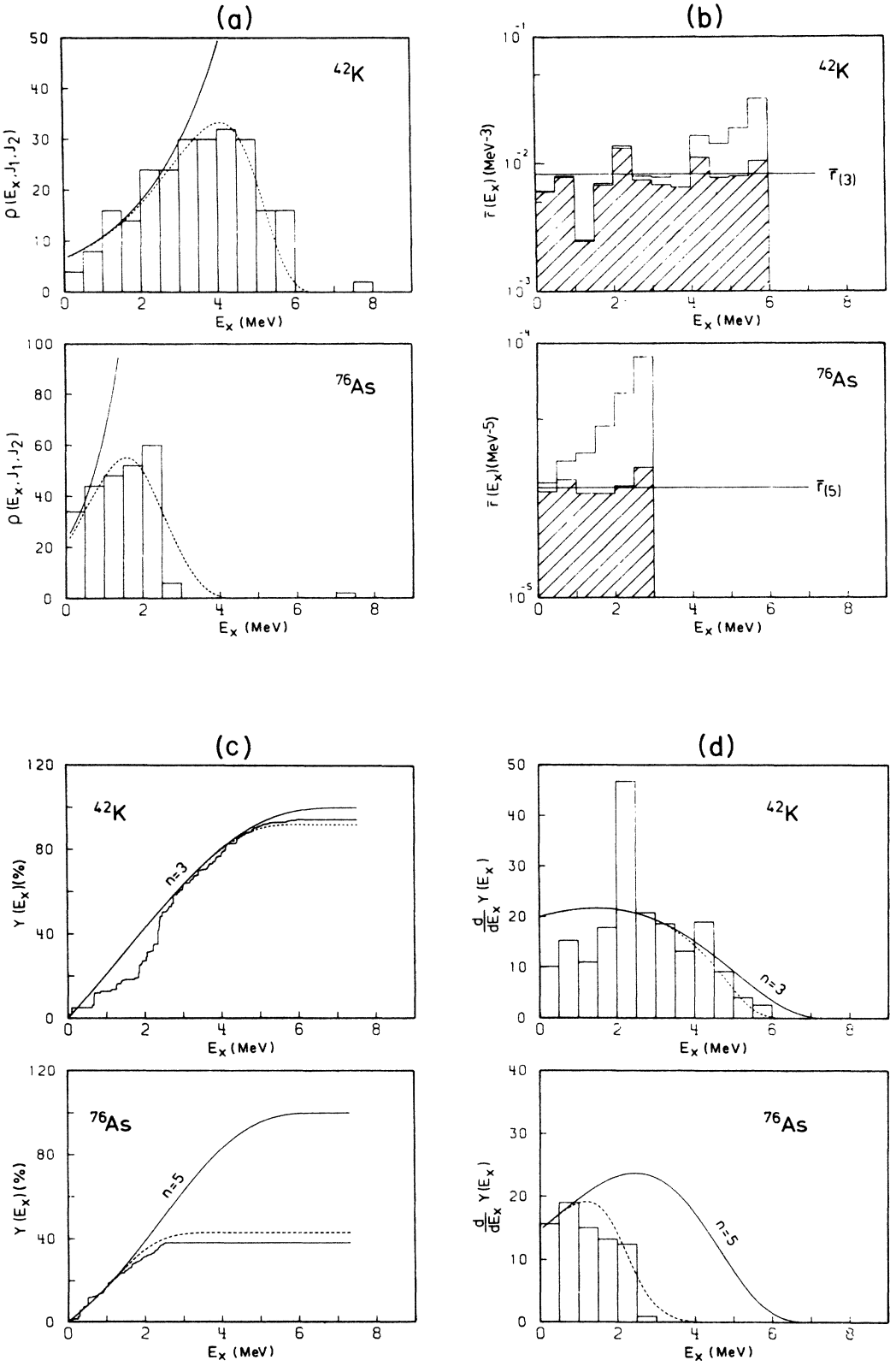

FIG. 5. Influence of detection corrections in ^{42}K and ^{76}As. (a) Level density $\rho(E_x,J_1,J_2)$. Histograms, experiment; solid lines, CTF fits; dashed lines, corrected CTF fits. (b) Average reduced intensities $\bar{r}(E_x)$. Histograms, experiment; hatched area, after correction. (c) and (d) Integrated and differential intensity $Y(E_x)$ and $dY(E_x)/dE_x$, respectively. Histograms, experiment; solid lines, statistical model prediction; dashed lines, statistical model prediction corrected for finite detection.

$$\bar{\Gamma}^{J^\pi}_{\gamma\lambda f}(E1)(\text{eV}) = \Gamma_w(E1)(\text{eV}) \equiv 6.8\times10^{-8} E_\gamma^3\,(\text{MeV}^3) A^{2/3} D_\lambda\,(\text{eV}) D_0^{-1}\,(\text{MeV}^{-1}) ,$$
$$\bar{\Gamma}^{J^\pi}_{\gamma\lambda f}(M1)(\text{eV}) = \Gamma_w(M1)(\text{eV}) \equiv 2.1\times10^{-8} E_\gamma^3\,(\text{MeV}^3) D_\lambda\,(\text{eV}) D_0^{-1}\,(\text{MeV}^{-1}) , \quad (21)$$

where D_λ is the average spacing of J^π resonances at energy E_λ, and D_0 is the single particle spacing. Throughout this paper the strengths of dipole transitions are expressed in Weisskopf units (W.u.) per MeV:

$$S_{X1}(\Gamma_{\gamma\lambda i}) D_0^{-1}(\text{W.u. MeV}^{-1}) = \frac{\Gamma_{\gamma\lambda i}}{\Gamma_w(X1) D_0\,(\text{MeV})} = \frac{I_\gamma(\%)\Gamma_\gamma}{100\Gamma_w(X1) D_0\,(\text{MeV})} . \quad (22)$$

Here, Γ_γ denotes the total radiative width and $\Gamma_{\gamma\lambda i}$ the partial width of a primary $X1$ transition with intensity I_γ.

Since the strengths of high energy $E1$ transitions in heavy nuclei are strongly influenced by the GDR,[37,42,45,46] their energy and mass dependence differ from the single particle estimate. Under the assumption that the same GDR is built on the ground state and each excited state,[36] $\bar{\Gamma}^{J^\pi}_{\gamma\lambda f}$ can be expressed in terms of the average total photoabsorption cross section $\bar{\sigma}_t(E_\gamma)$:

$$\bar{\Gamma}^{J^\pi}_{\gamma\lambda i}(E1) = \Gamma_{\text{GDR}}(E1) = \frac{1}{3\pi^2}\frac{1}{(\hbar c)^2} E_\gamma^2 \bar{\sigma}_t(E_\gamma) D_\lambda , \quad (23)$$

which yields the GDR prediction for the $E1$ strength,

$$S_{\text{GDR}}(E1) D_0^{-1} = \frac{\Gamma_{\text{GDR}}(E1)}{\Gamma_w(E1) D_0} . \quad (24)$$

In the present study the experimental $E1$ strengths are compared with several GDR approximations based on a Lorentzian shape of $\bar{\sigma}_t$:

$$\bar{\sigma}_t(E_\gamma) = \frac{\sigma_G \Gamma_G^2 E_\gamma^2}{(E_G^2 - E_\gamma^2)^2 + \Gamma_G^2 E_\gamma^2} . \quad (25)$$

Here, E_G, Γ_G, and σ_G denote the GDR energy, the width, and the peak cross section.

(i) Using $\Gamma_G = 5$ MeV, $E_G = 80 A^{1/3}$ MeV, and $\sigma_G = 13 A \Gamma_G^{-1}$ mb, Axel[36] obtained, for 6–8 MeV γ rays,

$$\bar{\Gamma}^{J^\pi}_{\gamma\lambda i} = 6.1\times10^{-15} E_\gamma^5\,(\text{MeV}^5) A^{8/3} D_\lambda\,(\text{eV}) . \quad (26)$$

(ii) The second approximation proposed by Schumacher *et al.*[42] uses the GDR parameters

$$\Gamma_G = 4.5 \text{ MeV} ,$$
$$E_G = 31.2 A^{-1/3} + 20.6 A^{-1/6} \text{ MeV} , \quad (27)$$
$$\tfrac{1}{2}\pi\sigma_G\Gamma_G = 72\ (\text{MeV mb}) NZA^{-1} .$$

(iii) As the investigated odd-odd isotopes are unstable, no experimental results on photoabsorption cross sections are available. However, the GDR parameter varies only smoothly with mass number, and thus another set of Lorentzian parameters was obtained from the measured photoabsorption[47] of the neighboring stable isotopes (see Table V).

It should be noted that for the light isotopes the Lorentzian shape of $\bar{\sigma}_t$ is a crude estimate.

For the $M1$ strengths a global expression in the frame of the GDR model is not yet available, although some results on the mass and energy dependence have been reported.[37,45,46] We therefore compare the $M1$ strengths to the semiempirical estimate proposed by Kopecky:[37]

$$\bar{\Gamma}^{J^\pi}_{\gamma\lambda f}(M1) = 9\times10^{-13} E_\gamma^5\,(\text{MeV}) A^{4/3} D_\lambda\,(\text{eV}) . \quad (28)$$

The experimental $E1$ and $M1$ strengths were calculated from Eq. (22) by averaging over proper energy bins. The resonance spacing D_λ was calculated from the CTF parametrization of the level density. Since, in general, thermal neutron capture does not proceed via a single resonance, we approximated the total radiative width Γ_γ by the average radiation width of s-wave resonances[32] in the energy region of the capture state (see Table V). It should be noted that the uncertainties hereby introduced to the absolute transition strengths do not affect the energy dependence of $E1$ and $M1$ strengths or the $E1/M1$ ratio discussed subsequently.

The assignment of primary dipole transitions to either $E1$ or $M1$ was done in the following way: For nuclei with $A \leq 42$ only the transitions to states with known parity

TABLE V. Total radiative width and GDR parameters.

		GDR parameters[b]		
Nucleus	Γ_γ (eV)[a]	E_G (MeV)	Γ_G (MeV)	σ_G (mb)
^{20}F	4.3(26)	24.0	10.0	13
^{24}Na	0.7(4)	24.0	12.0	12
^{28}Al	2.2(13)	21.8	8.0	15
^{32}P	3.1(19)	21.0	9.0	20
^{36}Cl	0.56(5)	21.2	10.5	27
^{40}K	2.0(12)	21.0	7.0	25
^{42}K	1.75(100)	21.0	7.0	25
^{46}Sc	0.84(46)	20.3	10.2	40
^{56}Mn	0.75(15)	18.0	7.0	65
^{60}Co	0.56(10)	18.0	7.0	75
^{64}Cu	0.50(10)	17.5	5.5	77
^{66}Cu	0.40(8)	17.0	7.0	77
^{72}Ga	0.24(7)	16.8	6.5	110
^{76}As	0.30(4)	16.3	7.4	95
^{80}Br	0.29(6)	16.5	6.5	135

[a] Average radiative width of s-wave neutron resonances (Ref. 32).

[b] Lorentzian parameters obtained from neighboring isotopes (Ref. 37).

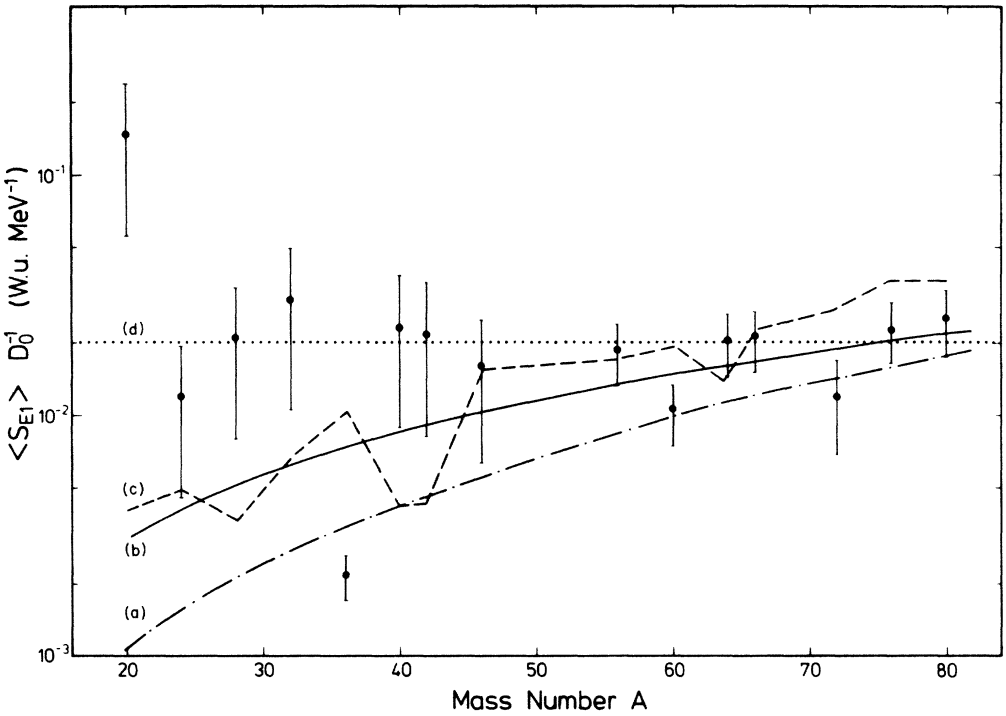

FIG. 6. $E1$ strengths averaged over all primary transitions to states in the region of completeness. The curves (a)—(c) are the GDR estimates (Axel's approximation, average, and individual Lorentzian parameters, respectively) calculated for a fixed energy $E_\gamma = 5.5$ MeV. The constant value (d) refers to 0.02 W.u. MeV^{-1}.

(see Table I) were included. For heavier nuclei parities are available only for few low lying states. Therefore, keeping in mind the higher relative intensities of $E1$ transitions in these nuclei, all primary transitions to states with unknown parity were given an $E1$ assignment. All $E1$ and $M1$ strengths discussed below were corrected for detection probability effects as outlined in Sec. IV.

B. Primary $E1$ strengths

The average $E1$ strengths $\langle S_{E1} \rangle D_0^{-1}$ of primary transitions to states in the complete regions (see Table IV) are displayed in Fig. 6 and compared with the three GDR estimates discussed in Sec. IV A and labeled (a)—(c). These predictions were evaluated from Eqs. (23)—(27) for the fixed energy $E_\gamma = 5.5$ MeV, which is near the centers of the energy regions involved. Even though the average GDR parameters [Eqs. (27)] differ considerably from those obtained from measured individual photoabsorption cross sections, both GDR estimates give similar results and fit the data better than Axel's approximation. However, the agreement of the experiment in the $A < 46$ nuclei with the GDR parametrization is poor and the experimental $E1$ strengths are systematically higher than the GDR prediction. Obviously, the $E1$ strengths are best described by the constant value $\langle S_{E1} \rangle D_0^{-1} = 0.02$ W.u. MeV^{-1}, corresponding to a retardation of a factor of 100 with respect to the Weisskopf estimate, with the single particle spacing $D_0 = 0.5$ MeV.

The $E1$ strengths averaged over 2 MeV wide energy bins are displayed in Fig. 7. Again, the average GDR estimates are given for comparison, calculated for the center of each bin, i.e., for $E_\gamma = 7$, 5, and 3 MeV. It is evident that the experimental values of $\langle S_{E1} \rangle D_0^{-1}$ behave very differently in the three energy bins: While they are well described by the GDR model in the 6—8 MeV bin, the strengths in the 4—6 MeV bin resemble Fig. 6 with constant strengths. Finally, in the 2—4 MeV bin a strong

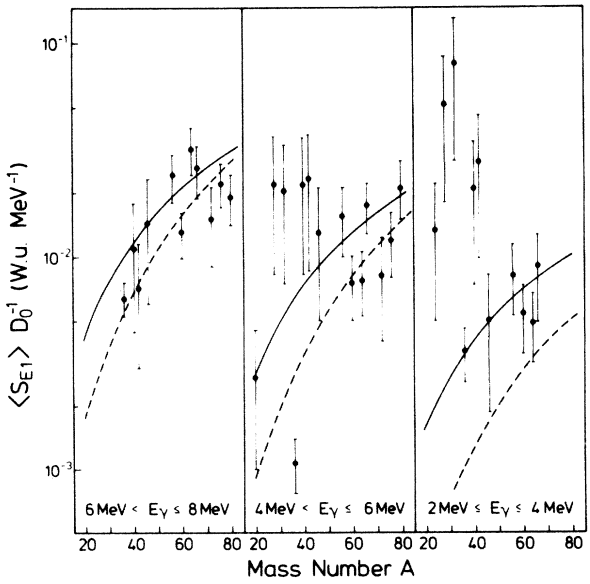

FIG. 7. $E1$ strength averaged over 2 MeV bins. The solid lines are the GDR predictions from Eq. (27); the dashed lines give the Axel estimate [Eq. (26)]. Theoretical values are calculated at the energy centers of each bin, i.e., at $E_\gamma = 7$, 5, and 3 MeV.

TABLE VI. Capture cross sections and distribution of spectroscopic factors.

Nucleus	σ_{th} (b)[a]	σ_D (b)[b]	$\sum S_{dp}(l_n=1)$ (%)[c] $6 \leqq E_\gamma \leqq 8$ MeV	$4 \leqq E_\gamma \leqq 6$ MeV	$2 \leqq E_\gamma \leqq 4$ MeV
^{20}F[d]	0.0096	0.0047	0	0	0
^{24}Na	0.53	0.0057	0	0	57
^{28}Al	0.231	0.108	0	28	71
^{32}P	0.172	0.110	0	22	70
^{36}Cl[e]	43.6				
^{40}K	2.1	0.753	0.1	54	46
^{42}K	1.46	1.32	7	69	24

[a] Thermal neutron capture cross sections (in barns) (Ref. 32).
[b] Direct capture cross sections at neutron energy $E_n = 25.3$ meV (in barns) (Ref. 32).
[c] Sum of $l_n = 1$ (l_n = neutron orbital angular momentum) spectroscopic factors to final states corresponding to the given energies of primary transitions (see text) (Refs. 48–52).
[d] All (d,p) $l_n = 1$ strength to states corresponding to $E_\gamma < 2$ MeV.
[e] Spectroscopic factors known only for $E_\gamma > 6$ MeV transitions.

peak occurs around $A \approx 30$, which exceeds the GDR estimate by an order of magnitude. This peak can be understood if one takes into account the direct capture process.[53] The GDR formalism does not apply to this type of reaction[54] and the strong $E1$ hindrance typical for the coupling to the GDR disappears.[55] In Table VI the thermal neutron cross sections σ_{th} of the light odd-A targets are compared to the total direct capture cross sections σ_D for 25.3 meV neutrons;[32] for all other nuclei direct capture is negligible. The typical feature of the direct capture mechanism is that the partial capture cross sections are proportional to the spectroscopic factors

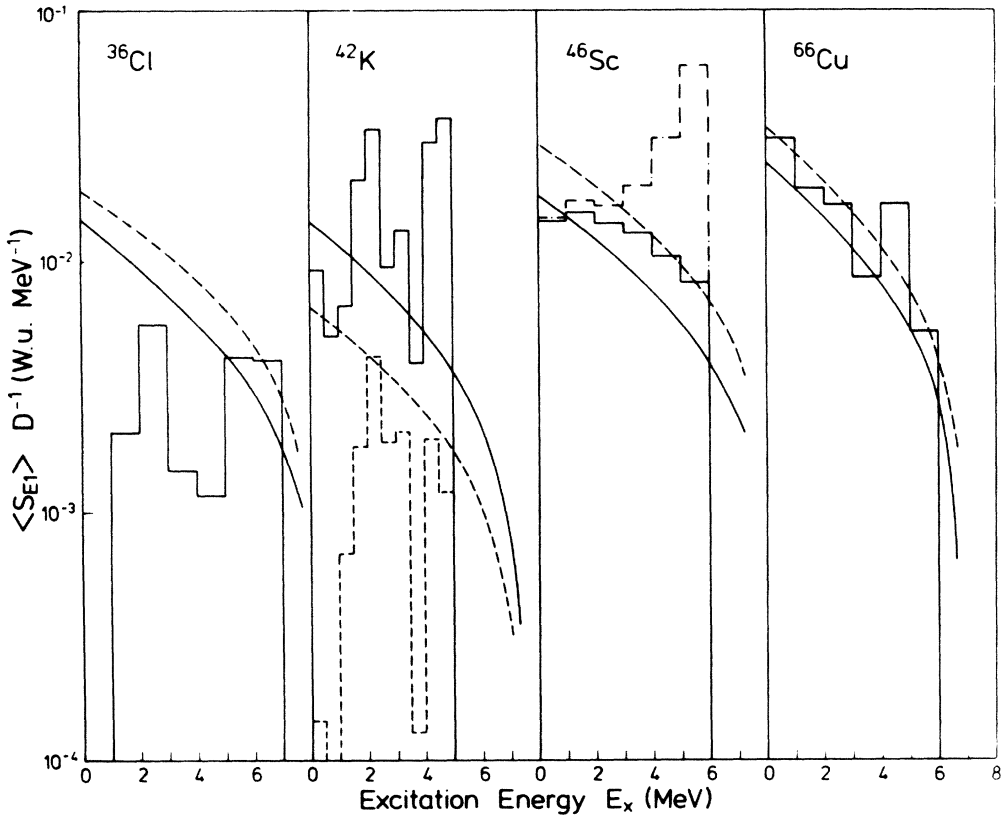

FIG. 8. Primary $E1$ strengths in ^{36}Cl, ^{42}K, ^{46}Sc, and ^{66}Cu as function of the excitation energy E_x of final states. The histograms refer to the experimental values; for ^{46}Sc the uncorrected experimental values are also given (dashed-dotted histogram). The solid lines are the GDR predictions with average Lorentzian parameters, while the dashed lines refer to the individual GDR parameters given in Table V. For ^{42}K the (d,p) $l_n = 1$ spectroscopic factors averaged over 0.5 MeV bins are indicated (dashed histogram) to demonstrate the influence of direct capture.

$S_{dp}(l_n=1)$ of p-wave neutron transfer via the (d,p) reaction. Table VI summarizes the sum of (d,p) $l_n=1$ spectroscopic factors to states in each energy bin of Fig. 7. The values are normalized to give $\sum S_{dp}(l_n=1)=100$, where the sum includes all states up to E_B. Comparison of Table VI and Fig. 7 shows that in almost all cases where direct capture is negligible, either because $\sigma_D \ll \sigma_{th}$ (i.e., in ^{36}Cl and all isotopes with $A \geqq 46$) or no final states with appreciable p-wave components are available, the experimental values of $\langle S_{E1}\rangle D_0^{-1}$ are in good agreement with the GDR prediction. On the other hand, significant contributions of direct capture always result in an enhancement proportional to this contribution.

Some selected examples for the energy dependence of $E1$ strengths given in Fig. 8 may illustrate this point. For ^{46}Sc and ^{66}Cu the agreement between the experimental values of $\langle S_{E1}\rangle D_0^{-1}$ and their GDR prediction is good, those with individual Lorentzian parameters fitting better than those with average GDR parameters. Agreement is also found for all other isotopes with $A \geqq 46$ [with the exception of ^{64}Cu (Refs. 9 and 39)]. On the other hand, the nucleus ^{42}K is a typical example for direct capture, the experimental strengths exceeding the GDR calculations by up to a factor of 20. No simple energy dependence appears (in average E_γ^3 rather than E_γ^5), but the strength is strongly structured and resembles the variation of (d,p) spectroscopic factors. The correlation between $E1$ strengths and spectroscopic $S_{dp}(l_n=1)$ factors is less than 0.02% by chance.

Finally, the isotope ^{36}Cl belongs to neither of the two groups. Even though part of the strength is roughly reproduced by the GDR estimate, no clear energy dependence is visible and in some regions the $E1$ transitions seem to be strongly hindered. The reason is that thermal neutron capture in ^{35}Cl proceeds almost entirely via a single 2^+ bound state resonance which gives rise to very specific features.

C. Primary $M1$ strengths

The average $M1$ strengths $\langle S_{M1}\rangle D_0^{-1}$ are displayed in Fig. 9 in the same way as the $E1$ strengths in Fig. 7. The 2–4 MeV energy bin was omitted because sufficient data are not available in that region. If one attempts to reproduce the data with a constant strength, one finds 0.2 W.u. MeV^{-1}, i.e., a much weaker hindrance than in the $E1$ case. However, the single particle model does not account for the observed A dependence of the average $M1$ strengths, which is better reproduced by the semiempirical GDR estimate, Eq. (28). At present, it is not possible to analyze the $M1$ strength in the heavier nuclei over a large enough energy range to differentiate between the single particle and GDR models because only a few $M1$ transitions have been identified so far. Consequently, one cannot verify the predicted energy dependence, as in the case of $E1$ transitions (Fig. 8).

The $M1$ strengths in the *sd* shell nuclei are displayed in Fig. 10 as a function of the excitation energy of the final states. The GDR estimate reproduces these results within the correct order of magnitude but does not account for the structured energy dependence of $\langle S_{M1}\rangle D_0^{-1}$. These

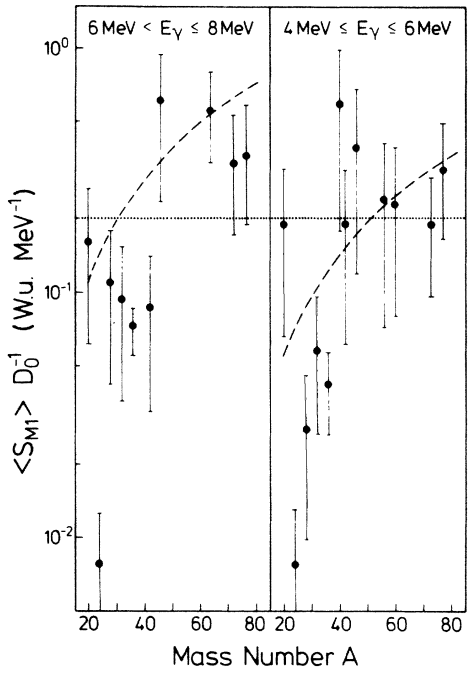

FIG. 9. $M1$ strength averaged over 2 MeV bins. The dashed curve refers to the semiempirical GDR estimate [Eq. (28)]. The dotted line corresponds to 0.2 W.u. MeV^{-1}.

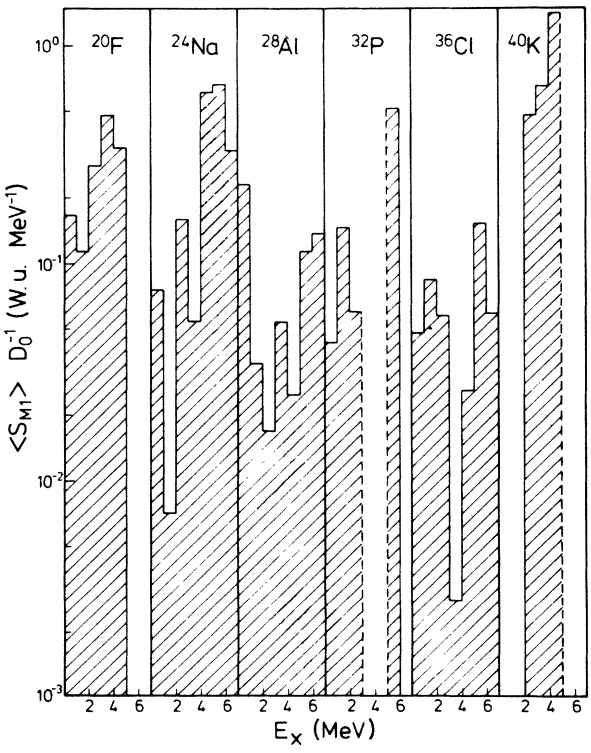

FIG. 10. $M1$ strength in *sd*-shell nuclei averaged over 1 MeV bins.

structure effects appear in a rather similar way in different nuclei, e.g., in ^{28}Al, ^{32}P, and ^{36}Cl. In these cases the capture process proceeds via different channels: only a $J^{\pi}=2^{+}$ bound state resonance for the reaction ^{35}Cl(n,γ)^{36}Cl, direct capture and a $J=0$ bound state resonance for ^{32}P, and direct capture and positive energy resonances for ^{28}Al. Thus these regularities are thought to reflect properties of the final states involved. Some of these features can be explained by simple shell model arguments, e.g., the strong change in the shape of the $M1$ spectra between ^{32}P, ^{36}Cl, and ^{40}K. For these nuclei the states accessible by primary $M1$ transitions must have positive parity (see Table I). Most of the low lying positive parity states in ^{32}P and ^{36}Cl have configurations in the *sd* shell.[56] On the other hand, low-lying 1p1h states in ^{40}K have $\pi(sd)^{-1}\nu(f_{7/2})^{1}$ negative parity configurations[57] and the low-lying positive parity states in this nucleus involve seniority $v=4$ 2p2h configurations. However, for a detailed understanding of these $M1$ distributions more elaborate shell model calculations are required.

D. $E1/M1$ ratio

The ratio of average $E1$ and $M1$ strengths can be deduced from the measured γ-ray intensities with much higher accuracy than the $E1$ and $M1$ strengths themselves, since the uncertainties of the radiation width Γ_{γ} and resonance spacing D_{λ} cancel and the uncertainty of the detection correction is reduced. On the other hand, this ratio is available only for a few combinations of γ energies and isotopes. The energy range is limited to high energies in the heavier isotopes since only few low energy $M1$ transitions are identified. In the *sd* shell nuclei, the positive and negative parity states are not equally distributed due to shell structure effects. For instance, in ^{24}Na, ^{28}Al, and ^{32}P, no negative parity states are available below 3 MeV. As the capture states have positive parity, no primary high energy $E1$ transitions exist for these isotopes. Figure 11 illustrates the integrated intensities of $E1$ and $M1$ transitions in ^{28}Al vs E_x. It is mainly this level density effect which brings about the disagreement between the dipole spectra of the *sd* shell nuclei and the statistical prediction (see Sec. III A, Fig. 3).

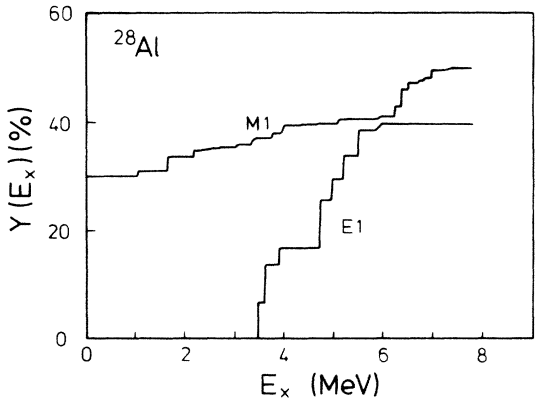

FIG. 11. Integrated intensity of primary $E1$ and $M1$ transitions in the ^{27}Al(n,γ)^{28}Al reaction.

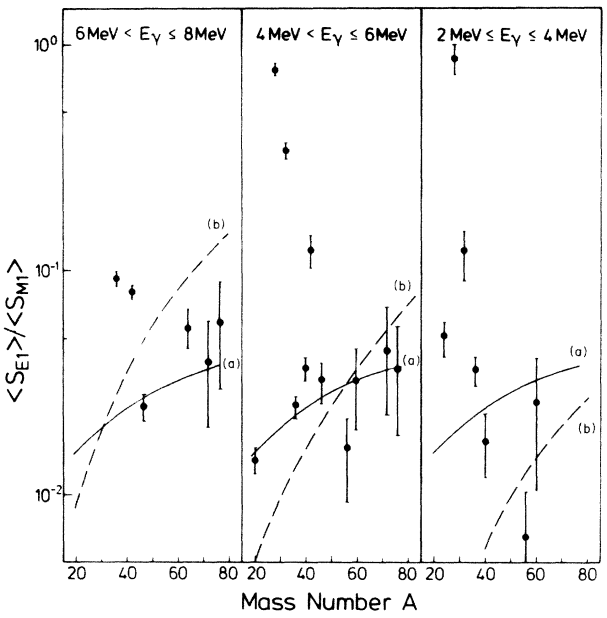

FIG. 12. Ratio of average $E1$ and $M1$ strengths as function of the mass number A, at the γ-ray energies given. Curve (a) refers to Axel's estimate of $E1$ strengths [Eq. (26)] and Kopecky's $M1$ GDR strength [Eq. (28)]. Curve (b) refers to a constant $M1$ strength of 0.2 W.u. MeV^{-1}.

The ratio of average $E1$ and $M1$ strengths for three different energy bins is displayed in Fig. 12 versus the mass number. The theoretical curves given are based on the assumptions that the $E1$ strengths are described by the GDR model, while for the $M1$ strengths either the GDR [curve (a)] or single particle estimate [$D_0=5$ MeV, curve (b)] is valid. Comparison to the data again favors the GDR estimate for the $M1$ strengths. The strong deviations for some light nuclei can be attributed to the enhancement of the $E1$ component by direct capture.

V. CONCLUSIONS

The present work represents a comprehensive analysis of the primary spectra in odd-odd nuclei in the mass range $20 \leqq A \leqq 80$ following thermal neutron capture. In agreement with the results of Ref. 29, which are based on a larger sample of (n,γ) data, we find that the level density in these nuclei up to several MeV of excitation can be well described by either the constant temperature Fermi gas model or the Bethe formula.[24] For the fitting parameters of both representations, we propose simple empirical relationships. The temperature parameter T of the CTF model shows a steplike mass dependence near the $A=40$ shell closure, similar to the single particle density parameter a in the Bethe formula. The deduced level schemes are essentially complete up to 1–5 MeV excitation energy.

Once the level densities are known, the average energy dependence and the fluctuations of the intensities of the primary spectra can be determined. Although the primary strengths follow Porter-Thomas distributions in all

investigated nuclei, the different energy scalings $\propto E_\gamma^n$ ($n=3,5$) point to distinct physical reasons dominating the spectra. These effects were analyzed on the basis of absolute transition strengths and the energy and mass dependence of $E1$ and $M1$ strengths. By properly correcting the γ-ray intensities for detection efficiency effects, dipole strengths were made available in energy regions up to several MeV in each nucleus.

The $E1$ strengths of nuclei with $A \geqq 46$ are in good agreement with the predictions of the giant dipole resonance model calculated from the photoabsorption cross sections. The energy and mass dependence of the $E1$ strength are indeed very well reproduced and the absolute $E1$ strengths are in satisfactory agreement, without the need of adjusting any parameter. The $E1$ strengths of the *sd*-shell isotopes, on the other hand, are enhanced with respect to the GDR predictions and show pronounced structures. Both effects are explained by direct neutron capture. We would like to emphasize, however, that even for these light nuclei the GDR model predicts reasonable results as long as the direct capture cross section is negligible. We thus conclude that the $E1$ spectra are essentially composed of a smoothly varying GDR component and a direct capture component which depends greatly on the level energy and mass number.

Concerning the primary $M1$ strengths, evidence is found for a slight mass dependence of its average strength and reasonable agreement with the empirical estimate by Kopecky.[37] However, in contrast to the $E1$ strengths, the present data do not allow one to verify the E_γ^5 dependence of the intensities predicted by the GDR ansatz, since only a few high energy $M1$ transitions could be identified in medium nuclei and strong nonstatistical effects were observed in the *sd*-shell nuclei which mainly reflect shell model structure effects of the final states.

In conclusion, the careful analysis of primary (n,γ) spectra provided information on the tails of the GDR in light nuclei as well as on shell model effects visible as direct neutron capture and/or the structure of final states. We would like to point out that although only primary transitions were included in the analysis, very detailed level schemes were required in order to identify primary transitions over a wide energy region, so as to test the energy dependence of strength functions. The major drawback in the analysis still arises from the insufficient knowledge of the parities of final states. The properties of the secondary spectrum of the (n,γ) process will be discussed, on the basis of Monte Carlo simulations, in a forthcoming paper.[43]

ACKNOWLEDGMENTS

The authors are grateful to T. von Egidy, H. A. Weidenmüller, P. Rullhusen, and M. Schumacher for stimulating discussions. The numerical analysis was carried out at the Gesellschaft für Wissenschaftliche Datenverarbeitung, Göttingen. This work was supported by Deutsches Bundesministerium für Forschung und Technologie.

---

*Present address: Institut Laue-Langevin, F-38042 Grenoble, France.

[1]P. Hungerford, T. von Egidy, H. H. Schmidt, S. A. Kerr, H. G. Börner, and E. Monnand, Z. Phys. A **313**, 339 (1983).

[2]P. Hungerford, T. von Egidy, H. H. Schmidt, S. A. Kerr, H. G. Börner, and E. Monnand, Z. Phys. A **313**, 325 (1983).

[3]H. H. Schmidt, P. Hungerford, H. Daniel, T. von Egidy, S. A. Kerr, R. Brissot, G. Barreau, H. G. Börner, C. Hofmeyr, and K. P. Lieb, Phys. Rev. C **25**, 2888 (1982).

[4]B. Krusche, K. P. Lieb, H. Daniel, T. von Egidy, G. Barreau, H. G. Börner, R. Brissot, C. Hofmeyr, and R. Rascher, Nucl. Phys. **A386**, 245 (1982).

[5]T. von Egidy, H. Daniel, P. Hungerford, H. H. Schmidt, K. P. Lieb, B. Krusche, S. A. Kerr, G. Barreau, H. G. Börner, R. Brissot, C. Hofmeyr, and R. Rascher, J. Phys. G **10**, 221 (1984).

[6]B. Krusche, Chr. Winter, K. P. Lieb, P. Hungerford, H. H. Schmidt, T. von Egidy, H. J. Scheerer, S. A. Kerr, and H. G. Börner, Nucl. Phys. **A439**, 219 (1985).

[7]T. A. A. Tielens, J. Kopecky, F. Stecher-Rasmussen, W. Ratynski, K. Abrahams, and P. M. Endt, Nucl. Phys. **A376**, 421 (1982).

[8]J. Kopecky, M. G. Delfini, and R. E. Chrien, Nucl. Phys. **A427**, 413 (1984).

[9]M. G. Delfini, J. Kopecky, J. B. M. DeHaas, H. I. Lion, R. E. Chrien, and P. M. Endt, Nucl. Phys. **A404**, 225 (1983).

[10]M. G. Delfini, J. Kopecky, R. E. Chrien, H. I. Lion, and P. M. Endt, Nucl. Phys. **A404**, 250 (1983).

[11]T. J. Kennett, W. V. Prestwich, and J. S. Tsai, Phys. Rev. C **32**, 2148 (1985).

[12]A. H. Colenbrander and T. J. Kennett, Can. J. Phys. **53**, 236 (1975).

[13]L. V. Johnson and T. J. Kennett, Nucl. Phys. **A113**, 104 (1968).

[14]H. Limusson, P. Hardell, and S. F. Arnell, Ark. Fys. **40**, 197 (1970); J. Vervier and H. H. Bolotin, Phys. Rev. C **3**, 1570 (1971).

[15]Do Huu Phuoc, R. Chery, H. G. Börner, W. F. Davidson, J. A. Pinston, R. Roussille, K. Schreckenbach, H. R. Koch, H. Seyfarth, and D. Heck, Z. Phys. A **286**, 107 (1978); Do Huu Phuoc, Ph.D. thesis, Université Claude Bernard, 1977.

[16]P. M. Endt and C. van der Leun, Nucl. Phys. **A310**, 331 (1978).

[17]R. L. Auble, Nucl. Data Sheets **24**, 25 (1978).

[18]R. L. Auble, Nucl. Data Sheets **20**, 275 (1977).

[19]M. L. Halbert, Nucl. Data Sheets **28**, 216 (1979).

[20]N. J. Ward and F. Kearns, Nucl. Data Sheets **36**, 184 (1982).

[21]F. Kearns and J. N. Mo, Nucl. Data Sheets **39**, 31 (1983).

[22]B. Singh and D. A. Viggars, Nucl. Data Sheets **31**, 137 (1980).

[23]B. Singh and D. A. Viggars, Nucl. Data Sheets **42**, 299 (1984).

[24]H. A. Bethe, Rev. Mod. Phys. **9**, 69 (1937).

[25]T. Ericson, Adv. Phys. **9**, 425 (1960).

[26]A. Gilbert and A. G. W. Cameron, Can. J. Phys. **43**, 1446 (1965).

[27]J. R. Huizenga, H. K. Vonach, A. A. Katsanos, A. J. Gorski, and C. J. Stephan, Phys. Rev. **182**, 1149 (1969).

[28]W. Dilg, W. Schantl, H. Vonach, and M. Uhl, Nucl. Phys. **A217**, 269 (1973).
[29]T. von Egidy, A. N. Behkami, and H. H. Schmidt, Nucl. Phys. **A454**, 109 (1986).
[30]Claude Bloch, Phys. Rev. **93**, 1094 (1954).
[31]B. Krusche, Ph.D. thesis, Universität Göttingen, 1985 (unpublished).
[32]S. F. Mughabgbab and D. I. Garber, Brookhaven National Laboratory Report No. BNL-325, 1973; S. F. Mughabgbab, M. Divadeenam, and N. E. Holden, *Neutron Cross Sections* (Academic, New York, 1981), Vol. 1, Pt. A.
[33]J. A. Holmes, S. E. Woosley, W. A. Fowler, and B. A. Zimmermann, At. Data Nucl. Data Tables **18**, 305 (1976).
[34]G. Rohr, Z. Phys. A **318**, 299 (1984).
[35]J. M. Blatt and V. F. Weisskopf, *Theoretical Nuclear Physics* (Wiley, New York, 1952).
[36]P. Axel, Phys. Rev. **126**, 671 (1962).
[37]J. Kopecky, in Proceedings of the 4th International Symposium on Neutron Capture γ-Ray Spectroscopy and Related Topics, Grenoble (1981), p. 423.
[38]C. E. Porter and R. G. Thomas, Phys. Rev. **2**, 483 (1956).
[39]W. E. Stein, B. W. Thomas, and R. E. Rae, Phys. Rev. C **1**, 1468 (1970).
[40]T. A. Brody, J. Flores, J. B. French, P. A. Mello, A. Pandey, and S. S. M. Wong, Rev. Mod. Phys. **53**, 385 (1981).
[41]J. J. M. Verbaarschot, Ph.D. thesis, Rijksuniversiteit Utrecht, 1982 (unpublished); J. J. M. Verbaarschot and P. J. Brussard, Phys. Lett. **87B**, 155 (1979).
[42]M. Schumacher, U. Zurmühl, F. Smend, and R. Nolte, Nucl. Phys. **A438**, 493 (1985).
[43]B. Krusche and K. P. Lieb, to be published.
[44]G. A. Bartholomew, E. D. Earle, A. J. Ferguson, J. W. Knowles, and M. A. Lone, Adv. Nucl. Phys. **7**, 229 (1974).
[45]Carol M. McCullagh, M. L. Stelts, and R. E. Chrien, Phys. Rev. C **23**, 1394 (1981).
[46]M. Aslam Lone, Proceedings of the 4th International Symposium on Neutron Capture γ-Ray Spectroscopy and Related Topics, Grenoble (1981), Ref. 37, p. 161.
[47]B. L. Berman, At. Data Nucl. Data Tables **15**, 319 (1975).
[48]F. Ajzenberg-Selove, Nucl. Phys. **A392**, 137 (1983).
[49]C. Daum, Nucl. Phys. **45**, 273 (1963).
[50]T. P. G. Carola and J. G. van der Baan, Nucl. Phys. **A173**, 414 (1971); S. Chen, J. Rapaport, H. Enge, and W. W. Buechner, *ibid.* **A197**, 97 (1972).
[51]T. Holtebekk, Nucl. Phys. **37**, 353 (1962).
[52]H. A. Enge, E. J. Irwin, Jr., and D. H. Weaner, Phys. Rev. **115**, 949 (1959).
[53]J. Lichtenstadt, A. Marinov, M. Paul, J. Burde, and S. Mordechai, Nucl. Phys. **A311**, 61 (1978).
[54]A. M. Lane and J. E. Lynn, Nucl. Phys. **17**, 563 (1960); **17**, 586 (1960).
[55]T. Uchiyama and H. Morinaga, Z. Phys. A **320**, 273 (1985).
[56]J. B. McGrory and B. H. Wildenthal, Annu. Rev. Nucl. Part. Sci. **30**, 383 (1980).
[57]M. F. Thomas, C. K. Davis, G. D. Jones, H. G. Price, and P. J. Twin, J. Phys. A **7**, 1985 (1974).